

Magnetism of the geometrically frustrated spin-chain compound $\text{Sr}_3\text{HoCrO}_6$: Magnetic and heat capacity measurements and neutron powder diffraction

V. Hardy, C. Martin, and G. Martinet

Laboratoire CRISMAT, UMR 6508, Boulevard du Maréchal Juin, F-14050 Caen Cedex, France

G. André

LLB, CEA-Saclay, F-91191 Gif-Sur-Yvette Cedex, France

(Received 23 May 2006; revised manuscript received 12 July 2006; published 16 August 2006)

This paper reports on the complex magnetic properties of $\text{Sr}_3\text{HoCrO}_6$, which is a spin-chain compound subject to geometrical frustration. This experimental study is based on magnetization and heat capacity measurements, combined with neutron powder diffraction. Our investigations provide evidence of a long-range antiferromagnetic ordering, taking place at $T_N \approx 15$ K. We focus on the nature of this magnetic ordering in zero field, as well as on the characteristics of the magnetization process at $T < T_N$. Particular attention is paid to the hysteresis loops recorded at $T \ll T_N$, which exhibit a peculiar succession of magnetization steps.

DOI: [10.1103/PhysRevB.74.064413](https://doi.org/10.1103/PhysRevB.74.064413)

PACS number(s): 75.60.-d, 75.45.+j

I. INTRODUCTION

The oxides of general formula $A'_3\text{ABO}_6$ provide us with a wide family of spin-chain compounds, which has been the subject of intense investigations in recent years. In this series of compounds, A' can be either Ca, Sr, or Ba, while the A and B sites can be occupied by a great variety of cations, including transition metals and rare-earth elements.¹ The rhombohedral structure of $A'_3\text{ABO}_6$ consists of $[\text{ABO}_6]_\infty$ infinite chains running along the c axis of the corresponding hexagonal cell, with the A' cations located in between them. These chains are made of alternating, face-sharing AO_6 trigonal prisms and BO_6 octahedra. Each chain is surrounded by six equally spaced neighbors forming a triangular lattice in the ab plane. The intrachain A - B separation is quite small (less than 0.3 nm in all cases), whereas the interchain distance is approximately twice that distance. Reinforcing this geometrical anisotropy, the oxygen atoms along the chains can efficiently mediate the intrachain coupling, which is not the case for the interchain coupling through the A' cations. These compounds are thus expected to display a pronounced one-dimensional (1D) magnetic character.

Particular attention has been paid to some compounds containing cobalt on the A site, like $\text{Ca}_3\text{Co}_2\text{O}_6$ (Refs. 2–19) or $\text{Ca}_3\text{CoRhO}_6$.^{20–25} These compounds share the same combination of features, which leads to geometrical frustration when considering a triangular lattice: (i) ferromagnetic intrachain coupling; (ii) antiferromagnetic interchain coupling; (iii) strong uniaxial anisotropy favoring the orientation of the spins along the chain direction.²⁶ Various unusual features were detected in the physical properties of these compounds. For instance, magnetic susceptibility and heat capacity measurements as well as neutron powder diffraction have suggested the achievement of a partially disordered antiferromagnetic (PDA) state²⁷ at temperatures lower than the Néel temperature (T_N), in $\text{Ca}_3\text{Co}_2\text{O}_6$ (Refs. 4, 6, and 8) and $\text{Ca}_3\text{CoRhO}_6$.^{20–25} Furthermore, in the case of $\text{Ca}_3\text{Co}_2\text{O}_6$, the curves of magnetization as a function of the magnetic field at $T \ll T_N$ exhibit a puzzling succession of rounded steps, whose spacing in field is approximately constant.^{5,6,11,13}

The origin of this latter phenomenon is still a matter of controversy. We have shown that various experimental results support the picture that this feature might be the manifestation of the phenomenon of quantum tunneling of the magnetization (QTM).^{11,13,15} Roughly speaking, this effect corresponds to the occurrence of increases in the rate of spin flipping through the anisotropy barrier (tunneling process), taking place for regularly spaced values of the magnetic field.²⁸ More recently, another interpretation has been proposed, invoking field-driven transitions between different local arrangements of spin-up and spin-down chains.¹⁹

It is worth pointing out that, at the present time, such a peculiar shape of $M(H)$ curves has only been clearly identified in $\text{Ca}_3\text{Co}_2\text{O}_6$, a fact that raises questions about the possible role of the presence of cobalt cations as the magnetic entities. It is well known, indeed, that the magnetism of compounds containing cations like Co^{3+} can be particularly complex owing to features such as the competition between different spin states or the existence of a substantial orbital contribution. Therefore, in order to address the existence of a possible relationship between the presence of steps on the $M(H)$ curves and the nature of the magnetic cations, we decided to investigate the occurrence of a similar phenomenon in a cobalt-free compound.

Following our idea of a QTM process, we focused on compounds presenting the basic ingredients for such a phenomenon: (i) strong uniaxial single-ion anisotropy; (ii) large spin values; (iii) ferromagnetic intrachain coupling; (iv) antiferromagnetic interchain coupling. In order to get large spin values, one can think of rare-earth (R) elements like Ho^{3+} or Dy^{3+} . In the literature, we found an extensive study of the series Sr_3RCrO_6 by Smith *et al.*²⁹ It was reported that the compound with $R=\text{Ho}$ was the only one to exhibit a ferromagnetic intrachain coupling. Furthermore, other results in the literature indicate that, for Ho^{3+} in an axially distorted trigonal prismatic environment, the crystalline electric field tends to generate a large uniaxial anisotropy.^{30–33} All these reasons made $\text{Sr}_3\text{HoCrO}_6$ seem an interesting candidate for the investigation of anomalous magnetic behavior. The results of the previous study of $\text{Sr}_3\text{HoCrO}_6$ only dealt with

neutron powder diffraction at room temperature and the temperature dependence of the susceptibility,²⁹ but no data were reported about many other aspects such as the $M(H)$ curves. We have thus carried out a detailed reinvestigation of the magnetic properties of the compound $\text{Sr}_3\text{HoCrO}_6$.

II. EXPERIMENTAL DETAILS

Polycrystalline samples of $\text{Sr}_3\text{HoCrO}_6$ were prepared by solid state reaction, starting from the oxides SrO , Ho_2O_3 , and Cr_2O_3 , which were weighted in the stoichiometric ratio (3:0.5:0.5) in a glovebox. Note that SrO was obtained from $\text{Sr}(\text{OH})_2 \cdot 8\text{H}_2\text{O}$ heated at 800°C in air for several days. After a thorough mixing of the precursors, the powder was pressed in the form of bars which were then heated at 1200°C for 12 h in evacuated ampoules.

X-ray powder diffraction was carried out at room temperature using a Philips diffractometer with $\text{Cu } K\alpha$ radiation. Energy-dispersive spectroscopy (EDS) was carried out to determine the actual cationic composition of our samples. This study was performed using a JEOL 200 CX equipped with a KeveX analyzer.

The neutron diffraction experiments were performed at LLB Saclay (France) by using the G4.1 diffractometer ($\lambda = 0.24266$ nm). A sample was first cooled down to 1.5 K and diffraction patterns were recorded in the angular range $6^\circ < 2\theta < 86^\circ$ at different temperatures. The spacing in temperature between successive recordings was ≈ 2 K in the range 1.5–25 K, and ≈ 10 K in the range 30–300 K. The data were then analyzed with the FULLPROF suite.³⁴

Magnetic measurements were carried out using an extraction magnetometer (PPMS, Quantum Design). The dc magnetization data were recorded in the temperature range $2 < T < 300$ K with a measuring field of 0.1 T, while the isotherms were measured in fields up to 9 T. The ac magnetic susceptibility was measured using an excitation field of 10 Oe at various frequencies in the range 10 – 10^4 Hz. Heat capacity measurements were carried out using a relaxation method (PPMS, Quantum Design), in zero field and for temperatures in the range $2 < T < 200$ K. In order to evaluate the lattice contribution, we also measured an isostructural, non-magnetic compound ($\text{Sr}_3\text{ZnPtO}_6$), whose preparation procedure and physical characterization were reported elsewhere.³⁵

III. RESULTS AND DISCUSSION

A. Structural characterizations

The x-ray pattern at 300 K shows that our $\text{Sr}_3\text{HoCrO}_6$ ceramics are almost single phased (about 95 wt %). As in the previous study,²⁹ however, the presence of a small amount of SrHo_2O_4 was identified [see Fig. 1(a)]. Several attempts to synthesize the pure compound without SrHo_2O_4 were not successful. In order to quantify the impact on the data, we synthesized a pure sample of SrHo_2O_4 . It was found that SrHo_2O_4 is paramagnetic down to 2 K, as demonstrated by (i) a linear temperature dependence of the reciprocal susceptibility and (ii) $M(H)$ curves showing a Brillouin shape at low T . As will be discussed below, it turns out that

accounting for the presence of this impurity phase improves the agreement between the data and our expectations. However, because of the uncertainty in the exact value of the SrHo_2O_4 fraction, we preferred to present the analysis without any corrections, and just mention how the results are modified if one takes into account the presence of this impurity (considering 5 wt %).³⁶

The structural characterization of the main phase $\text{Sr}_3\text{HoCrO}_6$ was performed on the basis of the neutron powder diffraction (NPD) recorded at 300 K. The refinement of the neutron diffraction data in the $R\bar{3}c$ space group leads to $a=0.97802(8)$ and $c=1.13063(9)$ nm. These values are in line with the previous results reported by Smith *et al.*²⁹ The structure of $\text{Sr}_3\text{HoCrO}_6$ consists of chains, running along the c axis, alternating face-shared HoO_6 prisms and CrO_6 octahedra, the Sr cations lying between the chains [see Figs. 1(b) and 1(c)]. The intrachain Ho-Cr distance is found to be 0.2827 nm, while the interchain distances are 0.5725 nm ($\times 6$) for Ho-Cr and 0.5953 nm ($\times 6$) for Ho-Ho or Cr-Cr. The octahedra are smaller than the prisms, having an average Cr-O distance of 0.2030 nm against 0.2255 nm for Ho-O [see Fig. 1(c)]. Even though the present data recorded with G4.1—a medium-resolution diffractometer—do not allow an accurate structural refinement, they clearly reveal the presence of a small amount of Cr on the Ho site. This feature is confirmed by the direct EDS analysis, which gives an average cationic composition close to $\text{Sr}_3\text{Ho}_{0.9}\text{Cr}_{1.1}$. Note that such an excess of Cr in the main phase is compatible with the existence of a small amount of SrHo_2O_4 as impurity.

B. Magnetic susceptibility

The main panel of Fig. 2 shows the temperature dependence of the susceptibility, which was recorded in 0.1 T following two different procedures: (i) the sample is cooled down to 2 K in zero field, then the field is applied, and the data are recorded upon warming up to 300 K [zero-field-cooled (ZFC) curve]; (ii) the magnetic field is applied at 300 K, then the data are recorded upon cooling down to 2 K [field-cooled (FC) curve]. The most salient features of Fig. 2 are (i) a flattening of the $\chi(T)$ curves over a small temperature range situated above 15 K; (ii) a well-defined kink at $T \approx 15$ K, followed by a steep rise as T is decreased further; (iii) a rounded maximum around 5 K (more pronounced on the ZFC curve), roughly corresponding to the appearance of the separation between the ZFC and FC curves at the lowest temperatures. It turns out that this set of features is very similar to what is observed in the case of $\text{Ca}_3\text{Co}_2\text{O}_6$ and $\text{Ca}_3\text{CoRhO}_6$,^{4,6,22–24} except that the kink in these compounds is located close to 26 and 90 K, respectively. One can also notice that the same behavior is found in $\text{Sr}_3\text{NiIrO}_6$, a compound of the $A'_3\text{ABO}_6$ family in which the intrachain coupling between Ni^{2+} ($S=1$) and Ir^{4+} ($S=1/2$) is antiferromagnetic.³⁷

According to these previous studies, the present behavior of the susceptibility curves of $\text{Sr}_3\text{HoCrO}_6$ can be associated with the following magnetic features: (i) the flattening of $\chi(T)$ as T is decreased toward 15 K can be ascribed to the development of antiferromagnetic interchain fluctuations; (ii)

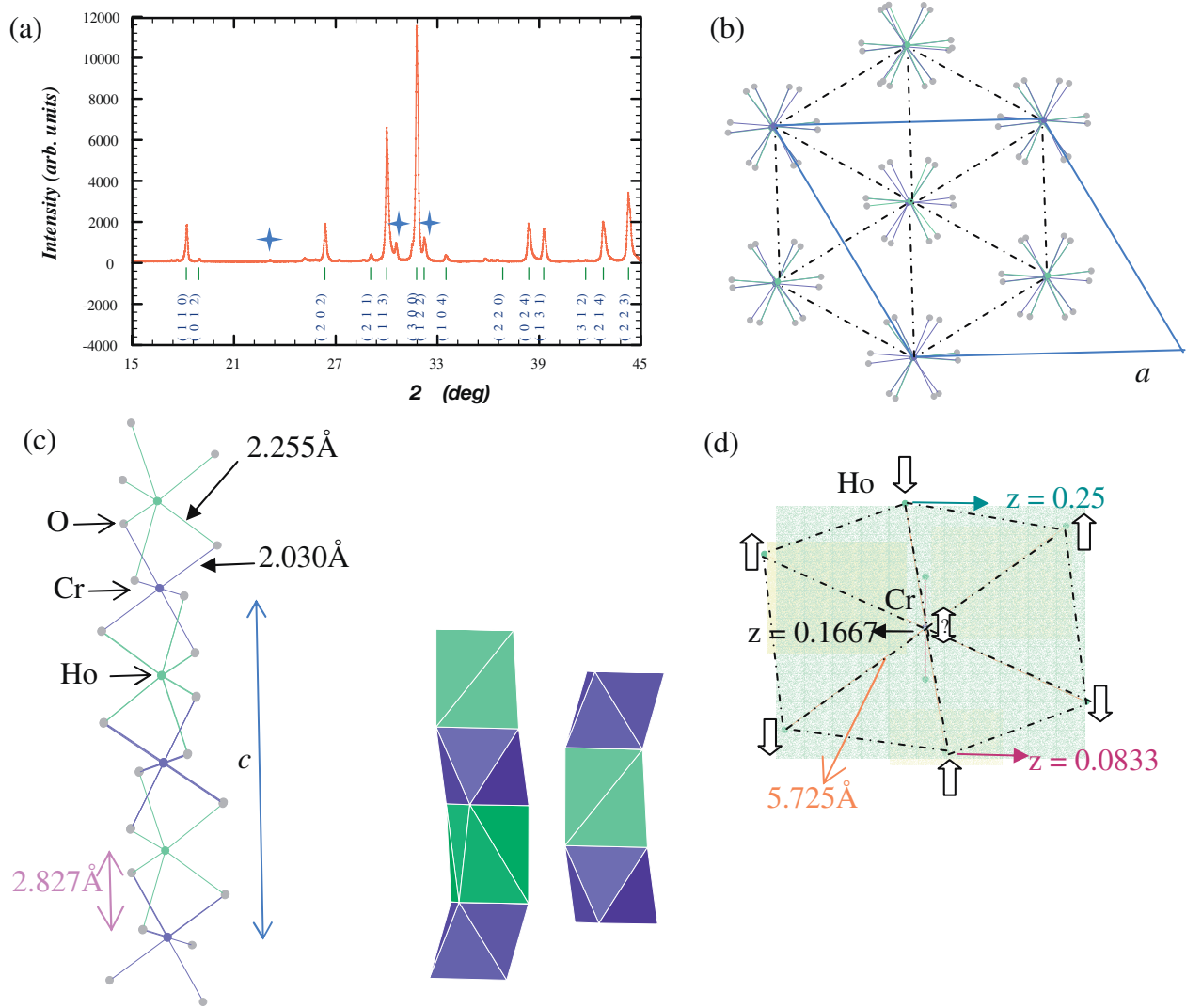


FIG. 1. (Color online) (a) Room-temperature x-ray pattern, indexed in the $R\bar{3}c$ space group; the stars correspond to the impurity SrHo_2O_4 . Drawings of the $\text{Sr}_3\text{HoCrO}_6$ structure: (b) projection in the basal plane to show the hexagonal structure and (c) along the c axis to evidence the 1D character of the structure. The solid lines indicate the unit cell and the dotted lines the triangular sublattice. Some interatomic distances (Cr-O, Ho-O, and intrachain Cr-Ho) are given. The HoO_6 and CrO_6 polyhedra are also shown. (d) corresponds roughly to (b) but details are added concerning the proposed magnetic structure.

the kink at 15 K would then correspond to the setting of a three-dimensional (3D) long-range magnetic ordering, driven by the combination of the inter- and intrachain couplings; even though this transition is basically antiferromagnetic, the susceptibility increases sharply as T is decreased below $T_N=15$ K because the establishment of a 3D ordering allows the intrachain ferromagnetic coupling to manifest itself;⁸ (iii) the behavior at lower temperatures, e.g., the separation between the ZFC and FC curves in the range 5–10 K, as well as the peaked shape of the ZFC $\chi(T)$ can be attributed to a spin-freezing phenomenon. This last feature is confirmed by the frequency dependence of the ac susceptibility, as shown in Fig. 3. One observes that increasing the frequency shifts the maximum found in both $\chi'(T)$ and $\chi''(T)$ to higher

temperatures. These shifts are particularly pronounced and similar to those previously observed in the $A_3^2\text{ABO}_6$ compounds that were claimed to undergo such a freezing in the PDA state. Associating the freezing temperature (T_f) with the peak in $\chi''(T)$, one derives a parameter $K=(\Delta T_f/T_f)/\Delta \log_{10} f$ which is ≈ 0.175 . This value is in line with those found in $\text{Ca}_3\text{Co}_2\text{O}_6$ (≈ 0.17),⁶ $\text{Ca}_3\text{CoRhO}_6$ (≈ 0.10),²² and $\text{Sr}_3\text{NiIrO}_6$ (≈ 0.12).³⁷

It is worth noticing that the existence of a kink at 15 K in $\chi(T)$ was not reported in the previous study of Smith *et al.*²⁹ A careful look at their data, however, suggests the presence of an anomaly in this T range, but it was hardly detectable because of a large Curie-like contribution, most probably associated with impurities or broken chains. Moreover, we

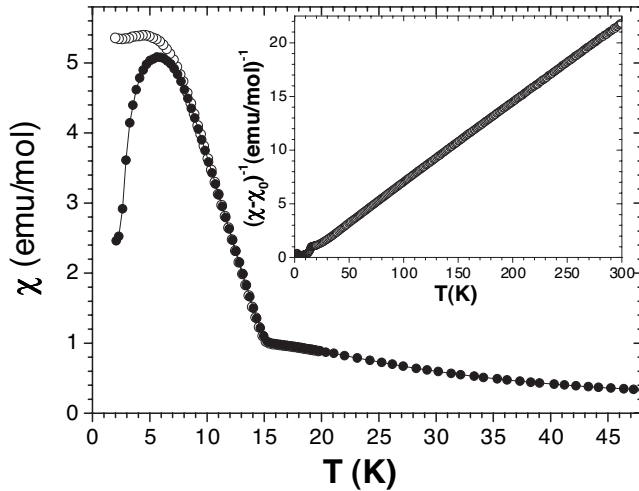


FIG. 2. dc magnetic susceptibility recorded with a magnetic field of 0.1 T, in the ZFC (filled circles) and FC (open circles) modes. The inset displays the T dependence of the reciprocal susceptibility (after subtraction of a constant term χ_0) over the whole T range (see text).

checked that the application of a high magnetic field (e.g., 0.5 T in Ref. 29) is not favorable to the observation of the kink at T_N , and it also tends to cancel the hysteresis between the ZFC and FC curves.

In the paramagnetic regime, i.e., for $T \gg T_N$, one observes a Curie-Weiss regime of the form $\chi = \chi_0 + C/(T - \theta)$, where C and θ are the Curie constant and the Curie-Weiss temperature, respectively, while χ_0 is a constant. The inset of Fig. 2 shows the reciprocal susceptibility after subtraction of a temperature-independent susceptibility $\chi_0 = 0.007$ emu/mol. When fitting to the data in the range 150–300 K, one derives $C \approx 13.57$ emu K/mol and $\theta \approx +3.3$ K.³⁸ The positive value of the latter parameter demonstrates the ferromagnetic nature of the intrachain coupling, consistently with the finding of Smith *et al.* ($\theta \approx +4.4$ K).²⁹ It can also be noted that this

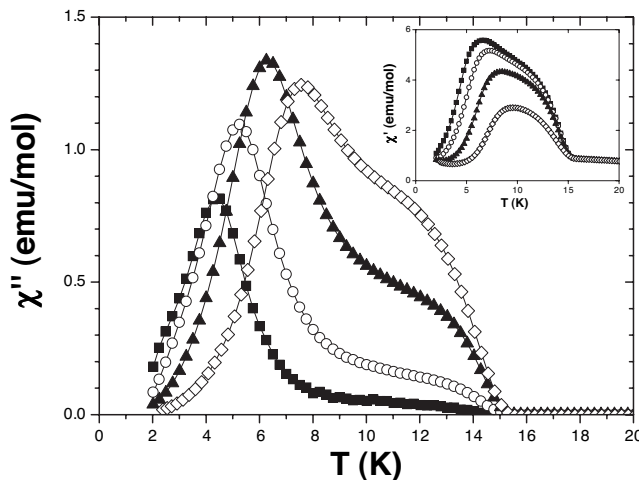


FIG. 3. Imaginary and real parts of the ac magnetic susceptibility (main panel and inset, respectively), recorded in zero dc field at various frequencies: 10 (filled squares), 10^2 (open circles), 10^3 (filled triangles), and 10^4 Hz (open diamonds).

value of θ is significantly smaller than the one found in $\text{Ca}_3\text{Co}_2\text{O}_6$, i.e., $\approx +30$ K (ceramic samples).³ This difference reveals that the intrachain ferromagnetic coupling J is much smaller in $\text{Sr}_3\text{HoCrO}_6$ than in $\text{Ca}_3\text{Co}_2\text{O}_6$. In spin-chain systems, the 3D long-range magnetic ordering takes place at a critical temperature which is a combination of the intra- and interchain couplings, i.e., J and J' , respectively. The larger are these couplings, the higher is the critical temperature. Accordingly, the observation of a T_N value that is lower in $\text{Sr}_3\text{HoCrO}_6$ than in $\text{Ca}_3\text{Co}_2\text{O}_6$ is consistent with the existence of a smaller J in the former compound, as well as a J' which is also probably smaller since the interchain distance is increased by the larger cationic radius of Sr^{2+} compared to Ca^{2+} .

Let us now turn to the analysis of the Curie constant. The effective number of Bohr magnetons per formula unit can be directly derived from the experimental Curie constant C through the relationship $p_{eff}^2 \approx 8C$, with C in emu K/mol. For a Cr^{3+} ion in an octahedral environment, one expects a quasispherical quench of the orbital contribution, leading to a spin-only behavior of the magnetic moment with $S=3/2$ and $g=2$.³⁹ For Ho^{3+} , the spin-orbit coupling is large, so the magnetic moment at high temperatures must be associated with the total angular momentum $J=8$ with a Landé factor $g_J=5/4$. Let us now compare the experimental value of p_{eff} with the theoretical expectation, taking into account the previously described nonstoichiometry between Cr and Ho. For the formula $\text{Sr}_3\text{Ho}_{1-x}\text{Cr}_{1+x}\text{O}_6$, the expected p_{eff} value is given by $p_{eff}^2 = (1+x)(2^2 \times \frac{3}{2} \times \frac{5}{2}) + (1-x)[(\frac{5}{4})^2 \times 8 \times 9]$. Combining this expression with the experimental value $p_{eff}^2 = 8C$, one can derive a quantitative estimate of the off-stoichiometry parameter $x = (255 - 16C)/195$, with C in emu K/mol. Using the experimental C value, one obtains $x \approx 0.19$, which is compatible with both the EDS and NPD data ($x \approx 0.1$), while it is also in very good agreement with the value reported by Smith *et al.* ($x = 0.196$) on the basis of their powder x-ray diffraction pattern.²⁹ Hereafter, we preferred to restrict ourselves to the results of the direct structural investigations, considering that the actual composition of our samples is close to “ $\text{Sr}_3\text{Ho}_{0.9}\text{Cr}_{1.1}\text{O}_6$ ”

C. Heat capacity

The main panel of Fig. 4 shows the temperature dependence of the zero-field heat capacity measured in $\text{Sr}_3\text{HoCrO}_6$, along with the data recorded in $\text{Sr}_3\text{ZnPtO}_6$, which is an isostructural nonmagnetic compound.³⁵ It must be emphasized that the curve of $\text{Sr}_3\text{HoCrO}_6$ clearly displays a peak close to 15 K, supporting the occurrence of a long-range magnetic ordering at this temperature, as suggested above by the susceptibility data. The magnetic contribution to the heat capacity of $\text{Sr}_3\text{HoCrO}_6$ [$C_{mag}(T)$] can be evaluated by subtracting the lattice contribution [$C_{ph}(T)$] from the raw data [$C(T)$]. The most reliable methods to estimate the phonon contribution of a magnetic material consist in using the data of an isostructural nonmagnetic compound [$C_{ref}(T)$], combined with an appropriate mass correction. To do so, we followed the procedure described by Bouvier *et al.*,⁴⁰ which is based on a rescaling of the Debye temperature. This

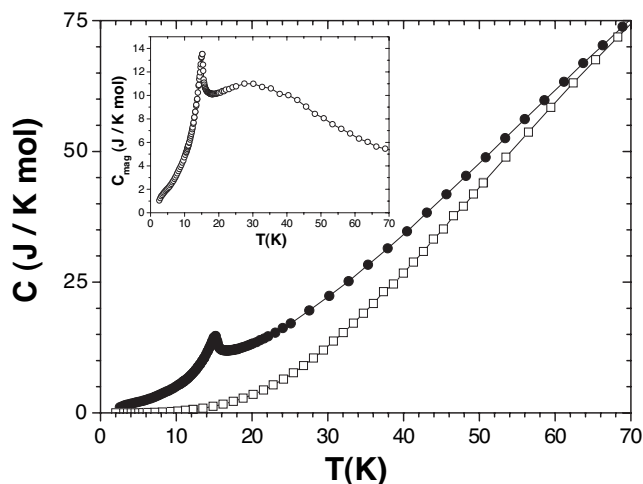


FIG. 4. Main panel: Total heat capacity of $\text{Sr}_3\text{HoCrO}_6$ (filled circles) and of $\text{Sr}_3\text{ZnPtO}_6$ (open squares). Inset: Magnetic heat capacity of $\text{Sr}_3\text{HoCrO}_6$, obtained after subtraction of the lattice contribution (see text).

method is supposed to be quantitatively correct at low temperature (i.e., below about 50 K in our case) which is precisely the T range relevant to the present study. Using Bouvier *et al.*'s method, the phonon contribution in $\text{Sr}_3\text{HoCrO}_6$ is calculated from the total heat capacity of the reference compound $\text{Sr}_3\text{ZnPtO}_6$ via the relationship $C_{ph}(T) = C_{ref}(T/r)$, where r is a function of the molecular weights of the various elements present in the two materials.⁴¹ In the present case, one finds $r = 1.045$.

The magnetic contribution to the heat capacity [$C_{mag}(T) = C(T) - C_{ph}(T)$] of $\text{Sr}_3\text{HoCrO}_6$ is shown in the inset of Fig. 4. One observes a sharp peak at $T \approx 15$ K—with a λ -like shape characteristic of a 3D long-range ordering—along with a rounded maximum located at higher temperatures (~ 30 K). This latter feature can be regarded as the manifestation of short-range magnetic fluctuations along uncoupled spin chains. The overall shape of the $C_{mag}(T)$ curve thus looks like the typical response of a quasi-1D system, in which weak interchain coupling leads to the setting of a 3D ordering at low temperatures.³⁹ As a matter of fact, it can be noted that the present result closely resembles the behavior found in $\text{CoCl}_2 \cdot 2\text{NC}_5\text{H}_5$, which is the prototypical example of a 1D Ising-like system having a ferromagnetic intrachain coupling.⁴² Furthermore, our data allow us to estimate the magnetic entropy S_{mag} by integrating C_{mag}/T . It is found that $S_{mag}(T \gg T_N)$ tends to a saturation around $\approx 30 \text{ J K}^{-1} \text{ mol}^{-1}$. In principle, for the actual composition $\text{Sr}_3\text{Ho}_{0.9}\text{Cr}_{1.1}\text{O}_6$, one should expect a maximum magnetic entropy equal to $R[0.9 \ln(17) + 1.1 \ln(4)] \approx 34 \text{ J K}^{-1} \text{ mol}^{-1}$. Taking the experimental uncertainties into account, one can consider that there is a good agreement between the theoretical and experimental values.

The most salient result of the heat capacity data is the confirmation that a 3D long-range magnetic ordering takes place in $\text{Sr}_3\text{HoCrO}_6$ close to 15 K. In order to go further into the characterization of this ordering, a neutron powder diffraction experiment was undertaken.

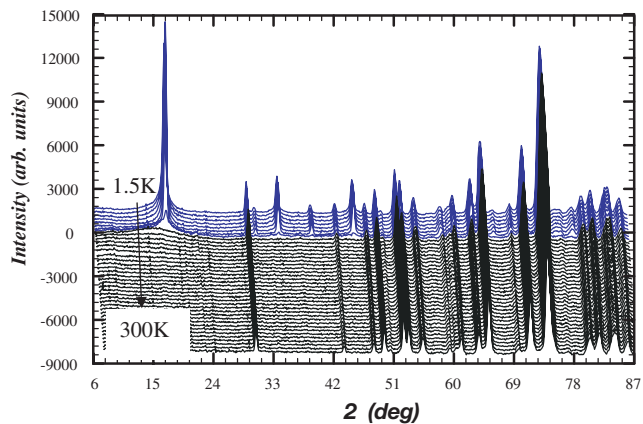


FIG. 5. (Color online) Neutron diffraction patterns, recorded from 1.5 to 300 K with $\lambda = 0.24266 \text{ nm}$. The gray (blue) and black colors are used for the magnetic ordered and paramagnetic states, respectively.

D. Neutron powder diffraction

The raw NPD patterns recorded from 1.5 to 300 K are shown in Fig. 5. First of all, it must be underlined that no structural transition is observed over the whole T range. The other main feature of this series of data is the appearance, for $T \leq 15$ K, of new peaks that are typical of a long-range antiferromagnetic ordering perpendicular to the hexagonal c axis. These NPD data thus clearly demonstrate that the transition temperature detected at ≈ 15 K in the physical properties is basically a Néel temperature T_N , associated with the onset of an antiferromagnetic ordering between the spin chains on the triangular lattice (ab plane). Besides, it must be specified that the temperature dependence of the intensity of the magnetic Bragg peaks is unusual, with a maximum at 9 K instead of 1.5 K, which suggests the appearance of magnetic disorder in this lower-temperature range. This is shown in Fig. 6(a) with the evolution of the most intense magnetic peak as a function of T .

This overall evolution of the NPD pattern as a function of T is in accordance with the previous studies reported in $\text{Ca}_3\text{Co}_2\text{O}_6$ (Ref. 3) and CaCoRhO_6 .^{20,21,25} To analyze more precisely the nature of the antiferromagnetic order taking place below 15 K in $\text{Sr}_3\text{HoCrO}_6$, we refined the NPD pattern at $T = 9$ K, which corresponds to the maximum of magnetic intensity, as shown in Fig. 6(b). It was found that the best fit corresponds to a magnetic model that is close to the one previously proposed for $\text{Ca}_3\text{Co}_2\text{O}_6$ and CaCoRhO_6 : two of the three chains on the triangular lattice [see Fig. 1(b)] are found to be ferromagnetically ordered—the moments lying along c —while the coupling between them is antiferromagnetic; the third chain remains incoherent, i.e., without long-range ordering of the spins. Let us now have a deeper insight into the environment of a Cr (Ho) atom belonging to this “incoherent” chain. As shown in Fig. 1(d), this Cr (Ho) is surrounded by six Ho (Cr) at the same distance (0.5725 nm), belonging to the six neighboring chains, but three Ho (Cr) are located “above” (making a triangle perpendicular to the c axis) while the three others are “below.” The apex of each triangle exhibits the same spin orientation along the c axis

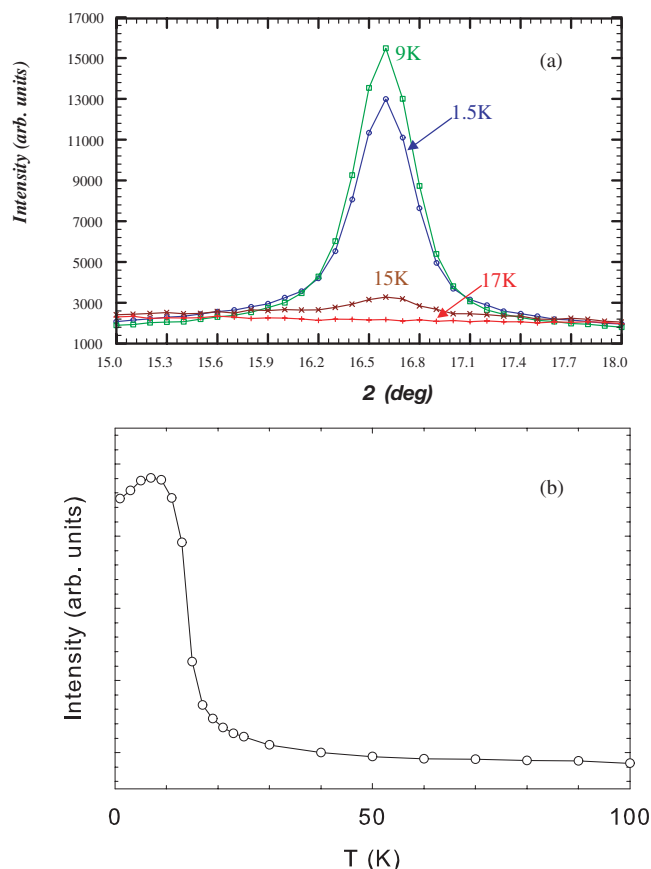


FIG. 6. (Color online) Enlargement of a few superimposed NPD patterns to illustrate the evolution vs T of the shape and intensity of the first magnetic peak (a) and corresponding integrated intensity—from 15 to 18 in 2θ —vs T (b).

(up or down), and this orientation is reversed from one triangle to the next, illustrating that the Cr (Ho) under consideration is in a typical situation of geometrical frustration.

All the characteristics of the antiferromagnetic order found in $\text{Sr}_3\text{HoCrO}_6$ are in agreement with previous reports about the realization of a PDA at low temperatures in this class of compounds. However, in contrast to what is observed for $\text{Ca}_3\text{Co}_2\text{O}_6$ or $\text{Ca}_3\text{CoRhO}_6$ (i.e., an almost zero magnetic moment on the octahedral sites), a nonzero magnetic moment is refined for each cation belonging to the magnetically ordered chains in the case of $\text{Sr}_3\text{HoCrO}_6$: $7.0\mu_B$ in the prisms and $2.0\mu_B$ in the octahedra.⁴³ For both sites, these values are lower than the expectations, i.e., $9.3\mu_B$ for the prisms (0.9 Ho+0.1 Cr) and $3\mu_B$ for the octahedra (1 Cr). Moreover, a careful comparison between experimental and calculated patterns shows that the magnetic peaks—in particular the first one—are not perfectly fitted by the model. In fact, there is a broad, weak contribution that is superimposed onto the standard (sharper) Bragg peak. A similar feature was reported by Loewenhaupt *et al.*²⁵ in their study of $\text{Ca}_3\text{CoRhO}_6$. The peak profile encountered in the present study can be accounted for by considering two magnetic components, both related to the same model, but with one of them corresponding to peaks of larger width. This procedure clearly improves the quality of the fit [see Fig. 7(a)], yielding

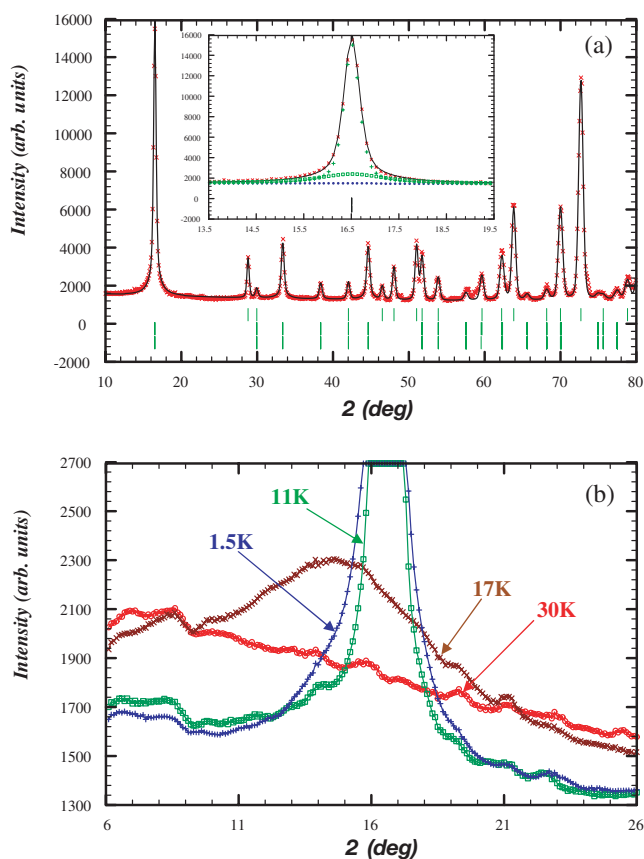


FIG. 7. (Color online) (a) Neutron diffraction pattern of $\text{Sr}_3\text{HoCrO}_6$ at 9 K. The crosses and the solid line correspond to the experimental and calculated diagrams, respectively. In the main panel, the upper Bragg ticks are for the crystalline structure, while the other sets of ticks correspond to the two magnetic contributions, which have the same magnetic structure but different coherence lengths (see text). The inset is an enlargement of the first peak showing the combination of these three contributions: crystalline contribution (\bullet), main magnetic contribution ($+$), and additional magnetic contribution having a shorter coherence length (\circ). The solid line is the sum of these three contributions, while the crosses are the data. (b) Enlargement of selected NPD patterns showing the evolution of the small-angle part vs temperature. For clarity the patterns have been smoothed.

somewhat larger values for the refined magnetic moment, i.e., $7.5\mu_B$ and $2.3\mu_B$ for Ho and Cr, respectively. Note that this procedure basically corresponds to the introduction of an additional short-range magnetic contribution (~ 4 nm of coherence length, to be compared with ~ 40 nm for the main contribution). It is also interesting to report that the coherence length of the main magnetic phase decreases when T is decreased from 9 down to 1.5 K, a feature consistent with the evolution of the magnetic Bragg peak displayed in Fig. 6(a).

The origin of the signal having a short coherence length is still unclear so far. It is likely, however, that it can be related to the particular structure of the spin system, which can be regarded as being arranged by sets of three chains, which are crystallographically equivalent, but corresponding to three different configurations of spins (the chains being either up,

down, or zero on average). Thereby, the presence of spin reversals along one of the chains may lead to variations in the spin configuration of the neighboring chains, inducing a short-range signature in the NPD patterns. Alternatively, the existence of a structure of diffuse magnetic peaks might be ascribed to short-range magnetic ordering developing along the incoherent chains, as previously proposed by Loewenhaupt *et al.*²⁵ in the case of $\text{Ca}_3\text{CoRhO}_6$.

Despite the improvement resulting from the combination of two peak profiles, a close inspection of the patterns shows that a lack of intensity remains in the small-angle side of the first magnetic peaks. To focus on this issue, enlargements of the small-angle part of a few patterns recorded at low T are displayed in Fig. 7(b). One observes that the background line at small angles ($2\theta < 12^\circ$) is strikingly enhanced for temperatures larger than T_N by about 10 K, with a maximum for $T=17$ K. This feature is reduced at lower temperatures, i.e., when the 3D long-range magnetic order occurs, but it is still present down to 1.5 K. It must be emphasized that the small-angle part of the NPD patterns is still far from being fully understood; clearly, this issue would deserve further investigations.

To summarize, the NPD patterns demonstrate that a large part of the spin system undergoes a 3D long-range antiferromagnetic ordering at $T_N \approx 15$ K involving two chains out of three, i.e., a picture compatible with the PDA. However, our data show that short-range magnetism also exists, including 3D and/or 1D components. The model presently used to fit the 9 K neutron diffraction data is based on a single type of 3D ordering, but it involves the coexistence of two characteristic lengths (yielding the superimposition of long- and short-range magnetic signals). It must be emphasized that 1D phenomena might also be taken into consideration.

E. Field dependence of the magnetization at $T < T_N$

Figure 8 shows a series of magnetization curves as a function of the magnetic field [$M(H)$], at different temperatures: $T=(a)$ 20 K $> T_N$; (b) 10 K $< T_N$; (c) 2 K $\ll T_N$. In each case, the $M(H)$ curve was recorded after zero-field cooling. At 20 K, the curve first shows a linear regime at low fields, then it progressively curves as the field is increased, suggesting the approach of the saturation magnetization. At 10 K, one observes something like a *distorted plateau* on the $M(H)$ curve in the low-field range (i.e., below ~ 1.5 T). At higher fields, the $M(H)$ curve recovers a rounded shape up to saturation. At 2 K, the $M(H)$ curve is hysteretic, in contrast to the two previous temperatures. In the first part of the curve (i.e., for fields lower than ~ 2 T), one can detect some modulations on both branches of the cycle. For higher magnetic fields, the curve progressively reaches saturation as at the previous temperatures.

Remarkably, this overall evolution of the $M(H)$ with temperature bears a striking similarity to the results found in $\text{Ca}_3\text{Co}_2\text{O}_6$.^{4-6,9} Considering these previous studies, the variation in the shape of $M(H)$ can be related to the different zero-field magnetic states existing in this class of compounds. For $T > T_N$ (e.g., 20 K), the $M(H)$ is linear in low fields, as simply expected for a paramagnetic regime. For

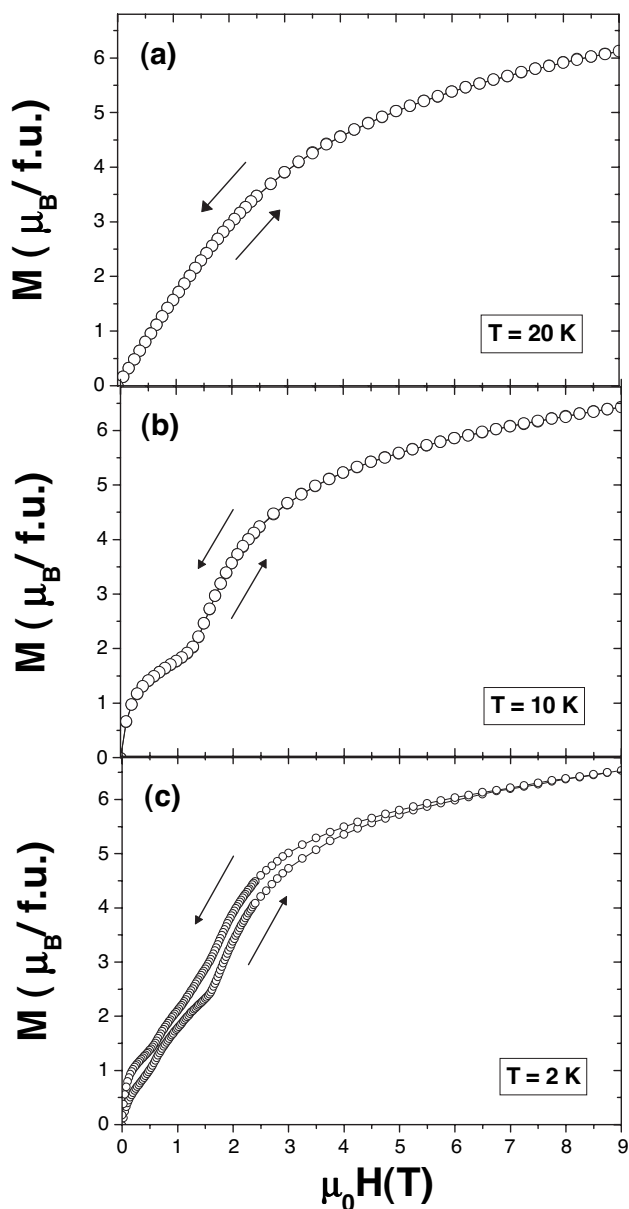


FIG. 8. Field dependence of magnetization curves recorded at three temperatures. The arrows indicate the direction of the field variation along the half loops.

$T < T_N$ (e.g., 10 K), the spin state after ZFC was reported to be a PDA state, where two-thirds of the chains are ferromagnetic with antiferromagnetic coupling between them, while the remaining third remains incoherent (disordered chains with zero net magnetization). As the field is applied, there is a transition toward a so-called ferrimagnetic state (consisting of ferromagnetic chains with two-thirds of them having spins up and one-third having spins down) manifesting itself as a plateau at one-third of the saturation magnetization M_{sat} . In a polycrystalline sample, the angular averaging smooths this magnetic response which basically corresponds to the configuration $H \parallel c$. Accordingly, the plateau expected for the ferrimagnetic state (i.e., with an almost constant magnetization at $M_{sat}/3$) is replaced by a shape similar to that found in Fig. 8(b). Finally, for $T \ll T_N$ (e.g., 2 K), the

compound is expected to be in a frozen-spin (FS) state, i.e., a state similar to the PDA state except that the dynamics of the spins—in particular those in the incoherent chains—is frozen. Such a FS state is at the origin of the hysteresis appearing at low T in the magnetic response, as well as other features such as a pronounced frequency dependence of the susceptibility. Moreover, in this regime of very low T , the $M(H\parallel c)$ recorded on single crystals of $\text{Ca}_3\text{Co}_2\text{O}_6$ shows a succession of magnetization steps.^{6,11,13} In ceramic samples, these underlying steps are found to generate discernible modulations in the $M(H)$ curves.^{4,9}

The origin of this phenomenon of magnetization steps in $\text{Ca}_3\text{Co}_2\text{O}_6$ has already been debated in the literature, but no consensus has emerged so far. It was early suggested that this phenomenon may be associated with the existence of various types of long-range ordering between spin-up and spin-down ferromagnetic chains.⁶ A recent neutron diffraction study performed on single crystals, however, has not supported this picture.¹⁷ Very recently, the appearance of steps in $M(H)$ was ascribed to the development of local arrangements of spin-up chains (the so-called *tripods*), whose density is controlled by entropy considerations.¹⁹ Previously, we had proposed another type of interpretation based on the phenomenon of quantum tunneling of the magnetization, affecting primarily the spins of the incoherent chains.^{11,13,15} It must be underlined that these last two interpretations can account for the occurrence of the steps at regularly spaced values of the magnetic field.

The analysis of the $M(H)$ curves shown in Fig. 8 is complicated by the fact that they have been recorded on a ceramic sample. In the case of $\text{Ca}_3\text{Co}_2\text{O}_6$ —the only member of this family of compounds for which single crystals are available—the direct comparison between data recorded on ceramics and on crystals with $H\parallel c$ (i.e., parallel to both the chains and the spins) clearly shows that the effect of angular averaging in a ceramic can profoundly spoil a number of features when the magnetic anisotropy is strong. For instance, the saturation magnetization of $\text{Ca}_3\text{Co}_2\text{O}_6$ ($M_{\text{sat}}=4.8\mu_B/\text{f.u.}$) is reached around 5 T at 10 K ($<T_N=26$ K) in single crystals,¹³ whereas the magnetization of a ceramic in the same conditions is only $1.7\mu_B/\text{f.u.}$, and it increases slowly till the highest magnetic field that was investigated (reaching $2.3\mu_B/\text{f.u.}$ in 9 T).

This issue raises the question of the magnetic anisotropy in $\text{Sr}_3\text{HoCrO}_6$. As in the case of $\text{Ca}_3\text{Co}_2\text{O}_6$, the anisotropy under consideration here is the single-ion anisotropy resulting from the crystalline electric field (CEF). On the one hand, one can state that Cr atoms located at octahedral sites are not expected to show anisotropic properties.³⁹ On the other hand, Ho^{3+} on prismatic sites may generate a pronounced anisotropy. In $\text{Sr}_3\text{HoCrO}_6$, each Ho^{3+} ion is surrounded by six O^{2-} forming a HoO_6 trigonal prism. It must be noted that the triangular faces of these prisms are shifted from each other by an angle $\approx 10.9^\circ$ around the c axis, leading to a CEF of trigonal dihedral symmetry (D_3). Even though there was no previous analysis of this particular situation, the literature provides us with various examples of CEF effects for Ho^{3+} in related anionic environments. Let us consider Ho^{3+} in CEF's having a trigonal symmetry. In all

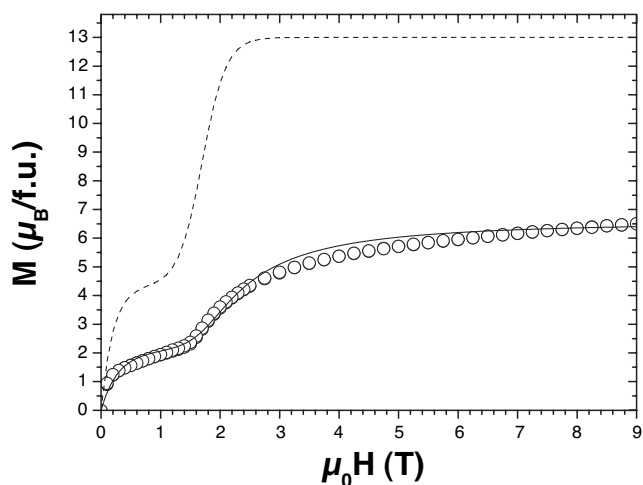


FIG. 9. Magnetization curve recorded at 5 K on a ceramic sample (open circles). The solid line is a fitting curve to the ceramic data, that is used to calculate the corresponding curve for a single crystal with $H\parallel c$ (dashed line), using our modelization (see the Appendix).

cases (C_{3v} in Ref. 30, C_{3h} in Ref. 31, D_{3d} in Ref. 33, as well as D_3 for nine nearest-neighboring oxygens in Ref. 32), the effect of the CEF on the 5I_8 multiplet of the free Ho^{3+} leads to a ground state that is a doublet. Since the energy spacing from the lowest-lying excited state(s) is quite large (larger than 15 cm^{-1} in all cases), one can consider that the ground-state doublet is the only populated state at very low temperatures such as $T=2$ K. This is a key point, since it was demonstrated by Griffith⁴⁴ that an isolated doublet of a non-Kramers ion (like Ho^{3+} which is $4f^{10}$) must lead to a giant anisotropy since the Landé factor perpendicular to the symmetry axis is equal to zero ($g_{\perp}=0$). A closer look at the examples of the literature with trigonal CEF's shows that, in all cases, the ground-state doublet is composed primarily of $|J_z=\pm 7\rangle$ or $|J_z=\pm 8\rangle$ states.³⁰⁻³³ Therefore, for Ho^{3+} in axially distorted trigonal CEF's, the magnetism at low T can be well approximated by considering magnetic moments associated with $J=8$, which are almost totally constrained to lie along the c axis.

According to the above discussion, it is reasonable to assume that the magnetic anisotropy of $\text{Sr}_3\text{HoCrO}_6$ is very large. It turns out that, in this limit, one can infer the magnetic response along the easy axis on the basis of ceramic data. The procedure to do so is described in the Appendix. It must be emphasized that, using the data of $\text{Ca}_3\text{Co}_2\text{O}_6$ (for which both ceramic and single-crystal data are available), it has been possible to directly confirm the reliability of this approach. Figure 9 shows, for $\text{Sr}_3\text{HoCrO}_6$ at $T=5$ K (reversible regime), the reconstruction of the underlying $M(H\parallel c)$ curve starting from the cycle that was measured on the ceramic sample. As compared to the ceramic data, the calculated $M(H\parallel c)$ curve exhibits a steeper rise after the plateau and it reaches a clearly field-independent saturation magnetization at $M_{\text{sat}}(H\parallel c)\sim 13\mu_B/\text{f.u.}$ We also note that if one considers the *crossing point* (see the Appendix) of the ceramic data, $M_{\text{cer}}^*\approx 2.2\mu_B/\text{f.u.}$, one also obtains a close value of $M_{\text{sat}}(H\parallel c)$, i.e., $\sim 13.2\mu_B/\text{f.u.}$ At this stage, it must be

emphasized that the present derivation of the $M(H\parallel c)$ curve is based on an oversimplification (infinite anisotropy) and is also subject to experimental uncertainties (illustrated by the imperfect fitting of the modelisation to the ceramic data). Keeping these reservations in mind, the obtained $M_{\text{sat}}(H\parallel c)$ values are well consistent with the theoretical expectations for $\text{Sr}_3\text{HoCrO}_6$. Indeed, the fully polarized moment of each Cr^{3+} is $2 \times 3/2 = 3\mu_B$, while for Ho^{3+} one can expect $5/4 \times 8 = 10\mu_B$. Therefore, the theoretical saturation magnetization for $\text{Sr}_3\text{HoCrO}_6$ is $13\mu_B/\text{f.u.}$, or $12.3\mu_B/\text{f.u.}$ if one considers the actual composition $\text{Sr}_3\text{Ho}_{0.9}\text{Cr}_{1.1}\text{O}_6$. Globally, there is a good consistency between the theoretical and the “experimental” values.⁴⁵

Unfortunately, the same technique cannot be used at very low temperatures (e.g., 2 K), essentially because the shape of the underlying $H\parallel c$ response in this T regime is more complex, and it can hardly be anticipated with enough accuracy. As a consequence, in order to estimate the $H\parallel c$ response of $\text{Sr}_3\text{HoCrO}_6$ in this temperature range, there is no other way than just trying to improve the degree of orientation of the measured samples. All our attempts to orientate powder in grease or epoxy, by applying large magnetic fields at room temperature (as it can be done in $\text{Ca}_3\text{Co}_2\text{O}_6$, for instance,^{5,8}) were unsuccessful. The failure of this technique may be attributed to a too weak anisotropy of the magnetic susceptibility at high temperatures. However, as discussed above, the magnetic anisotropy is expected to be very large at low temperatures. Therefore, another possible strategy would consist in using finely divided powder and apply a large magnetic field at very low T , in order to induce a rotation of the c axis of each grain toward the direction of the field. At such very low T , all host materials (like grease, etc.) are frozen, so the powder must be used alone. Thereby, the resulting powder alignment can only be partial and quite unstable, since it involves solid friction between the grains. In other respects, we had noticed in our previous study on $\text{Ca}_3\text{Co}_2\text{O}_6$ single crystals that the pattern of steps is more pronounced on the reverse leg of the $M(H)$ loops.¹³

Accordingly, we carried out the following procedure with $\text{Sr}_3\text{HoCrO}_6$: (i) a ceramic sample was finely ground in order to ensure that each particle is made of a single grain with a unique c -axis direction; (ii) this powder was put into a capsule without pressing it, in order to allow the maximum degrees of freedom for each grain to rotate; (iii) this sample was zero-field cooled down to 2 K; (iv) our maximum magnetic field of 9 T was slowly applied, and the magnetization was recorded as a function of the field while decreasing it down to zero. The result of such a procedure is shown in Fig. 10. One can immediately observe the existence of an alignment effect in that the magnetization values are substantially larger than those obtained on a ceramic. As a matter of fact, the magnetization in 2 T for instance is $\approx 5.9\mu_B/\text{f.u.}$ in the oriented powder, to be compared to $\approx 3.9\mu_B/\text{f.u.}$ in the ceramic (Fig. 8). On the other hand, it is likely that the alignment is not total, since the magnetization remains much lower than the calculated $M(H\parallel c) \approx 11\mu_B/\text{f.u.}$ value displayed in Fig. 9.⁴⁶ However, it is patent that these data on “partially oriented” powder enhances the signatures of the steps in the low-field range (see the arrows on Fig. 10).

These features are still more visible in the inset of Fig. 10, where is displayed the derivative of the $M(H)$ curve. Four

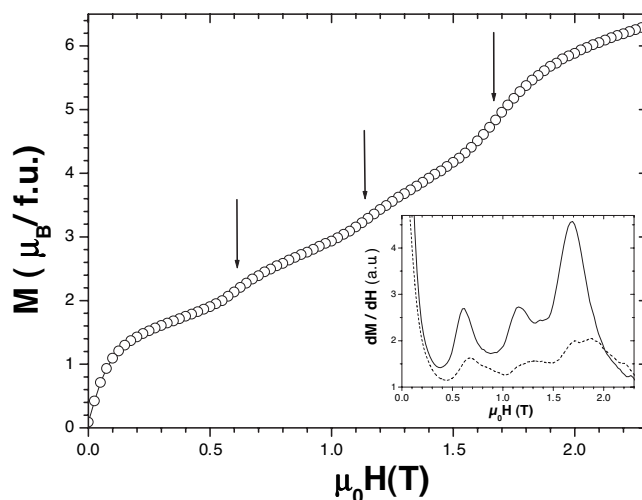


FIG. 10. Reverse leg of a half loop recorded at 2 K in a partially oriented powder sample (see text). The arrows indicate changes in slope that are more clearly visible in the derivative curve shown in the inset (solid line). The inset also displays the corresponding curve obtained in a randomly oriented ceramic sample (dashed line).

maxima clearly emerge for $\mu_0 H < 2$ T, approximately located at $\mu_0 H = 0$; 0.6; 1.15, and 1.7 T. One can notice that these characteristic fields correspond to an average spacing equal to 0.55 T. The inset also displays the derivative of the field-decreasing part of the $M(H)$ recorded at 2 K in a ceramic. The comparison of the two curves clearly shows that (i) the steps are more marked in the oriented powder, and (ii) the field values associated with the steps are shifted to lower values. Accordingly, one can speculate that the true characteristic fields that would be obtained in a perfectly oriented sample should be still a bit shifted to lower values, and could lead to a better constant spacing between them.

At this stage, it is difficult to go further in the analysis of these steplike features on the $M(H)$ curves. It can reasonably be stated, however, that this data on $\text{Sr}_3\text{HoCrO}_6$ strikingly resembles that previously reported in $\text{Ca}_3\text{Co}_2\text{O}_6$. This result shows that the observation of almost equally spaced characteristic fields in the latter compound was not coincidental, and it rather points to a sort of universal behavior within this class of compounds.

F. Conclusion

The spin-chain compound $\text{Sr}_3\text{HoCrO}_6$ has been investigated by combining magnetic and heat capacity measurements, as well as powder neutron diffraction. This study has provided a series of results about the magnetic properties of this compound. In particular, we found evidence of a 3D long-range antiferromagnetic order occurring at $T_N \approx 15$ K in $\text{Sr}_3\text{HoCrO}_6$. The NPD study showed that the magnetic state at $T < T_N$ has features consistent with PDA, a state that is theoretically expected in quasi-1D compounds experiencing geometrical frustration. Furthermore, $\text{Sr}_3\text{HoCrO}_6$ was found to exhibit the same intriguing properties as those previously observed in $\text{Ca}_3\text{Co}_2\text{O}_6$, another member of the $A_3\text{ABO}_6$

family. In particular, both compounds give rise to a puzzling pattern of steps on the $M(H)$ curves at low T .

First, one can state that the observation of magnetization steps in $\text{Sr}_3\text{HoCrO}_6$ demonstrates that this peculiar behavior—which was only observed in $\text{Ca}_3\text{Co}_2\text{O}_6$ so far—is not intrinsically related to the presence of Co in the spin chains. Second, the present results reinforce the idea that this behavior is linked to a specific set of features that is found in both $\text{Ca}_3\text{Co}_2\text{O}_6$ and $\text{Sr}_3\text{HoCrO}_6$: the presence of large spins with a strong uniaxial anisotropy, and the existence of a particular combination of intra- and interchain couplings (ferromagnetic and antiferromagnetic, respectively).

At the present time, two types of interpretation are in competition to account for the magnetization steps appearing at very low T in these spin-chain compounds: (i) a mechanism of quantum tunneling of the magnetization, involving primarily the spins located in the incoherent chains;^{11,15} (ii) entropy-driven excitations yielding local bunches of ferromagnetic spin-up chains.¹⁹ It was shown that each of these approaches can account for the main features of the phenomenon, including the almost constant spacing existing between the field steps. In order to test further the reliability of each of these models, the availability of new compounds presenting this phenomenon of magnetization steps is a point of crucial importance.

Accordingly, the results of the present study encourage further work on this topic: first, one should extend the investigations to other members of the $A_3'ABO_6$ family, in order to specify the exact requirements for the development of a multistep behavior in the magnetization process; second, for each compound displaying such a behavior, one should try to synthesize single crystals of large size, in order to perform complementary studies—like single-crystal neutron diffraction—allowing a more direct insight into the microscopic nature of the anomalous $M(H)$ curves at low T .

ACKNOWLEDGMENT

The authors thank M. Hervieu for the EDS analysis.

APPENDIX

Let us consider the following situation.

(1) Magnetization measurements are performed on a ceramic sample of a compound having a very large uniaxial anisotropy (with easy magnetization along a direction referred to as the c axis hereafter).

(2) This anisotropy is so large that one can consider that the magnetization vector always points along the c axis, and depends only on the magnetic field component that is oriented along this direction.

(3) The measurement technique is such that one only gets access to the component of the magnetization that is oriented along the direction of the applied field (referred to as the z axis hereafter).

$M_{cer}(H)$ is the magnetization curve that is measured on a ceramic sample made of randomly oriented grains. The present goal is to derive from these data the underlying

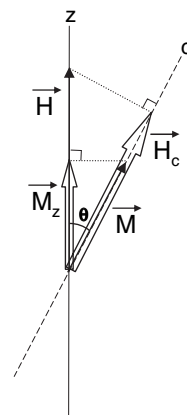


FIG. 11. Sketch of the vectorial projections used to calculate the contribution to the global magnetization of a grain whose c axis is tilted by an angle θ from the direction of the applied magnetic field (see the Appendix).

$M_{cry}(H)$ curve that would be obtained by measuring a single crystal with $H \parallel c$.

The orientation of the c axis of each grain can be defined by introducing the polar angles θ and φ with respect to the z axis. As depicted in Fig. 11, the contribution of each grain is obtained by considering first, the projection of the field along c ($H_c = H \cos \theta$) and second, the projection of the magnetization along z ($M_z = M \cos \theta$). The global response of a collection of randomly oriented grains is given by a standard angular average, leading to

$$M_{cer}(H) = \frac{1}{2\pi} \int_{\varphi=0}^{\varphi=2\pi} \int_{\theta=0}^{\theta=\pi/2} \cos \theta M_{cry}(H \cos \theta) \sin \theta d\theta d\varphi,$$

$$M_{cer}(H) = - \int_{\theta=0}^{\theta=\pi/2} \cos \theta M_{cry}(H \cos \theta) d(\cos \theta).$$

With $x = \cos \theta$, one obtains the basic relationship

$$M_{cer}(H) = \int_0^1 x M_{cry}(xH) dx. \quad (\text{A1})$$

Assuming a certain shape for $M_{cry}(H)$, it is possible to parametrize this function and then to derive the values of the parameters through Eq. (A1).

1. Derivation of $M_{cry}(H)$ from $M_{cer}(H)$

We have tested the validity of this approach in the case of $\text{Ca}_3\text{Co}_2\text{O}_6$, the only compound related to $\text{Sr}_3\text{HoCrO}_6$ for which both single-crystal and ceramic data are available. At intermediate-temperatures (e.g., $15 \text{ K} < T_N \approx 25 \text{ K}$), the measured $M_{cry}(H)$ curve rapidly reaches a first plateau at $\sim M_{sat}/3$ (ascribed to a ferrimagnetic state), before being switched to M_{sat} above $H_0 \approx 3.6 \text{ T}$ (ferromagnetic state).^{5,6,13} This field dependence can be correctly reproduced by the function

$$M_{cry}(H) = M_{sat} \left\{ \frac{1}{3} \left[1 - \exp\left(-\frac{H}{a}\right) \right] + \frac{2}{3} \left(\frac{1}{1 + \exp[-(H-H_0)/b]} \right) \right\}, \quad (\text{A2})$$

where a , b , H_0 and M_{sat} are adjustable parameters.

Using Eqs. (A1) and (A2) with the experimental $M_{cer}(H)$ of $\text{Ca}_3\text{Co}_2\text{O}_6$, one obtains a *calculated* $M_{cry}(H)$ that is found to be very close to the *measured* $M_{cry}(H)$, except that the value of M_{sat} is a bit lower in the latter case. Actually, we measured $M_{sat} \sim 4.8\mu_B/\text{f.u.}$,¹³ whereas the calculated value is $5.1\mu_B/\text{f.u.}$ It is worth noticing that the latter value is closer to recent predictions¹⁸ and experimental results from x-ray magnetic circular dichroism ($\sim 5.2\mu_B/\text{f.u.}$).⁴⁷ As noted by Wu *et al.*,¹⁸ it cannot be ruled out that a small disorientation is still present when using a set of single crystals, a situation which would lead to an underestimate of M_{sat} . Therefore, one can consider that the test of Eqs. (A1) and (A2) in the case of $\text{Ca}_3\text{Co}_2\text{O}_6$ globally supports the reliability of this approach.

2. Estimation of M_{sat} from M_{cer}^*

The function of Eq. (A2) cannot be integrated analytically, so in our test with $\text{Ca}_3\text{Co}_2\text{O}_6$, we had to use a numerical integration for Eq. (A1). However, if one limits oneself to

the low-field range [i.e., the first term of Eq. (A2)], the function can be solved exactly, leading to (for $H \ll H_0$)

$$M_{cer}(\alpha) = \frac{M_{sat}}{3} \left(\frac{1}{2} + \frac{e^{-\alpha}}{\alpha} + \frac{e^{-\alpha}}{\alpha^2} - \frac{1}{\alpha^2} \right),$$

where $\alpha = H/a$.

For $a \sim 0.2$ T as found in $\text{Ca}_3\text{Co}_2\text{O}_6$ (as well as in $\text{Sr}_3\text{HoCrO}_6$, when refining the complete function), it can be checked that α is large enough in the intermediate field range corresponding to the plateau (i.e., $\mu_0 H = 1-2$ T) to simply consider the approximation

$$M_{cer} \approx M_{sat}/6.$$

However, the magnetization plateau in ceramic samples is not as flat as for $H \parallel c$ in a crystal. The question thus arises: which magnetization value (M_{cer}^*) is the most relevant to the low-field plateau $H \ll H_0$? In the case of $\text{Ca}_3\text{Co}_2\text{O}_6$, we have observed that (i) for a crystal, the most accurate value of the magnetization at the plateau corresponds to the crossing point¹³ found between the $M_{cry}(H)$ curves recorded at different $T < T_N$; (ii) in a ceramic, this crossing point leads to a M_{cer}^* value that is found to be $\sim 1/6$ of the calculated M_{sat} .

As a consequence, another way to roughly estimate M_{sat} from ceramic data consists in (i) first, determining M_{cer}^* from the crossing point between curves at different T ; (ii) then, using the relationship $M_{sat} \approx 6M_{cer}^*$.

-
- ¹K. E. Stitzer, J. Darriet, and H.-C. zur Loye, *Curr. Opin. Solid State Mater. Sci.* **5**, 535 (2001).
- ²H. Fjellvag, E. Gulbrandsen, S. Aasland, A. Olsen, and B. Hauback, *J. Solid State Chem.* **124**, 190 (1996).
- ³S. Aasland, H. Fjellvag, and B. Hauback, *Solid State Commun.* **101**, 187 (1997).
- ⁴H. Kageyama, K. Yoshimura, K. Kosuge, H. Mitamura, and T. Goto, *J. Phys. Soc. Jpn.* **66**, 1607 (1997).
- ⁵H. Kageyama, K. Yoshimura, K. Kosuge, M. Azuma, M. Takano, H. Mitamura, and T. Goto, *J. Phys. Soc. Jpn.* **66**, 3996 (1997).
- ⁶A. Maignan, C. Michel, A. C. Masset, C. Martin, and B. Raveau, *Eur. Phys. J. B* **15**, 657 (2000).
- ⁷B. Raquet, M. N. Baibich, J. M. Broto, H. Rakoto, S. Lambert, and A. Maignan, *Phys. Rev. B* **65**, 104442 (2002).
- ⁸V. Hardy, S. Lambert, M. R. Lees, and D. McK. Paul, *Phys. Rev. B* **68**, 014424 (2003).
- ⁹S. Rayaprol, K. Sengupta, and E. V. Sampathkumaran, *Solid State Commun.* **128**, 79 (2003).
- ¹⁰R. Frésard, C. Laschinger, T. Kopp, and V. Eyert, *Phys. Rev. B* **69**, 140405(R) (2004).
- ¹¹A. Maignan, V. Hardy, S. Hébert, M. Drillon, M. R. Lees, O. Petrenko, D. McK. Paul and D. Khomskii, *J. Mater. Chem.* **14**, 1231 (2004).
- ¹²D. Flahaut, A. Maignan, S. Hébert, C. Martin, R. Retoux, and V. Hardy, *Phys. Rev. B* **70**, 094418 (2004).
- ¹³V. Hardy, M. R. Lees, O. A. Petrenko, D. McK. Paul, D. Flahaut, S. Hébert, and A. Maignan, *Phys. Rev. B* **70**, 064424 (2004).
- ¹⁴E. V. Sampathkumaran, N. Fujiwara, S. Rayaprol, P. K. Madhu, and Y. Uwatoko, *Phys. Rev. B* **70**, 014437 (2004).
- ¹⁵V. Hardy, D. Flahaut, M. R. Lees, and O. A. Petrenko, *Phys. Rev. B* **70**, 214439 (2004).
- ¹⁶D. Dai and M.-H. Whangbo, *Inorg. Chem.* **44**, 4407 (2005).
- ¹⁷O. A. Petrenko, J. Wooldridge, M. R. Lees, P. Manuel, and V. Hardy, *Eur. Phys. J. B* **47**, 79 (2005).
- ¹⁸H. Wu, M. W. Haverkort, Z. Hu, D. I. Khomskii, and L. H. Tjeng, *Phys. Rev. Lett.* **95**, 186401 (2005).
- ¹⁹Y. B. Kudasov, *Phys. Rev. Lett.* **96**, 027212 (2006).
- ²⁰S. Niitaka, H. Kageyama, K. Yoshimura, K. Kosuge, S. Kawano, N. Aso, A. Mitsuda, H. Mitamura, and T. Goto, *J. Phys. Soc. Jpn.* **70**, 1222 (2001).
- ²¹S. Niitaka, K. Yoshimura, K. Kosuge, M. Nishi, and K. Kakurai, *Phys. Rev. Lett.* **87**, 177202 (2001).
- ²²E. V. Sampathkumaran and A. Niazi, *Phys. Rev. B* **65**, 180401(R) (2002).
- ²³S. Niitaka, K. Yoshimura, K. Kosuge, A. Mitsuda, H. Mitamura, and T. Goto, *J. Phys. Chem. Solids* **63**, 999 (2002).
- ²⁴V. Hardy, M. R. Lees, A. Maignan, S. Hébert, D. Flahaut, C. Martin, and D. McK. Paul, *J. Phys.: Condens. Matter* **15**, 5737 (2003).
- ²⁵M. Loewenhaupt, W. Schäfer, A. Niazi, and E. V. Sampathkumaran, *Europhys. Lett.* **63**, 374 (2003).
- ²⁶*Magnetic Systems with Competing Interactions*, edited by H. T. Diep (World Scientific, Singapore, 1994); P. Schiffer and A. P. Ramirez, *Comments Condens. Matter Phys.* **18**, 21 (1996); A. P. Ramirez, in *Handbook of Magnetic Materials*, edited by K. J. H. Buschow (Elsevier, Amsterdam, 2001); S. T. Bramwell and M. P. Gingras, *Science* **294**, 1495 (2001).
- ²⁷M. Mekata, *J. Phys. Soc. Jpn.* **42**, 76 (1977); M. Mekata and K.

- Adachi, *ibid.* **44**, 806 (1978).
- ²⁸For a review, see *Quantum Tunneling of Magnetization*, edited by L. Gunther and B. Barbara (Kluwer, Dordrecht, 1995).
- ²⁹M. D. Smith and H.-C. zur Loye, *Chem. Mater.* **12**, 2404 (2000).
- ³⁰U. Ranon and K. Lee, *Phys. Rev.* **188**, 539 (1969).
- ³¹C. A. Catanese and H. E. Meissner, *Phys. Rev. B* **8**, 2060 (1973).
- ³²D. M. Moran, A. De Piantè, and F. S. Richardson, *Phys. Rev. B* **42**, 3317 (1990).
- ³³Y. M. Jana and D. Ghosh, *Phys. Rev. B* **61**, 9657 (2000).
- ³⁴J. Rodriguez-Carvajal, *Physica B* **192**, 55 (1993).
- ³⁵S. Majumdar, V. Hardy, M. R. Lees, D. McK. Paul, H. Rous-selière, and D. Grebille, *Phys. Rev. B* **69**, 024405 (2004).
- ³⁶The values of magnetization of $\text{Sr}_3\text{HoCrO}_6$ can be derived from the raw data either with or without the correction associated with the presence of ~ 5 wt % of SrHo_2O_4 (referred to as M_{cor} and M , respectively). Let us refer to M_{imp} as the magnetization measured in the pure sample of SrHo_2O_4 . Denoting by $\mathcal{M}(\text{Sr}_3\text{HoCrO}_6)$ and $\mathcal{M}(\text{SrHo}_2\text{O}_4)$ the molar masses of $\text{Sr}_3\text{HoCrO}_6$ and SrHo_2O_4 , respectively, the relationship between M_{cor} and M is $M_{cor} = (M/0.95) - \{(0.05/0.95) \times [\mathcal{M}(\text{Sr}_3\text{HoCrO}_6)/\mathcal{M}(\text{SrHo}_2\text{O}_4)]M_{imp}\}$. Here, we considered all the magnetizations as being molar quantities.
- ³⁷D. Flahaut, S. Hébert, A. Maignan, V. Hardy, C. Martin, M. Hervieu, M. Costes, B. Raquet, and J. M. Broto, *Eur. Phys. J. B* **35**, 317 (2003).
- ³⁸Correcting the data from the SrHo_2O_4 impurity leads to a smaller value of χ_0 (≈ 0.004 emu/mol), while it makes no significant changes to either C or θ .
- ³⁹L. J. De Jongh and A. R. Miedema, *Adv. Phys.* **23**, 1 (1974).
- ⁴⁰M. Bouvier, P. Lethuillier, and D. Schmitt, *Phys. Rev. B* **43**, 13137 (1991).
- ⁴¹Within the framework of the model proposed by Bouvier *et al.* (Ref. 40), the parameter r allowing us to calculate the lattice contribution in $\text{Sr}_3\text{HoCrO}_6$ from the data recorded in $\text{Sr}_3\text{ZnPtO}_6$ is $r = \{3[\mathcal{M}(\text{Sr})]^{3/2} + [\mathcal{M}(\text{Ho})]^{3/2} + [\mathcal{M}(\text{Cr})]^{3/2} + 6[\mathcal{M}(\text{O})]^{3/2} / 3[\mathcal{M}(\text{Sr})]^{3/2} + [\mathcal{M}(\text{Zn})]^{3/2} + [\mathcal{M}(\text{Pt})]^{3/2} + 6[\mathcal{M}(\text{O})]^{3/2}\}^{1/3}$, where $\mathcal{M}(X)$ is the molecular weight of the element X .
- ⁴²K. Takeda, S. Matsukawa, and T. Haseda, *J. Phys. Soc. Jpn.* **30**, 1330 (1971).
- ⁴³In the refinement, a zero value is assigned to the magnetic moment of the cations of the “disordered” chains (one out of three).
- ⁴⁴J. S. Griffith, *Phys. Rev.* **132**, 316 (1963).
- ⁴⁵Correcting the data from the SrHo_2O_4 impurity yields a smaller value of M_{sat} ($\approx 12.2\mu_B/\text{f.u.}$), which remains in good agreement with the theoretical values (it is even in better accordance with the expectation if one considers the actual composition $\text{Sr}_3\text{Ho}_{0.9}\text{Cr}_{1.1}\text{O}_6$).
- ⁴⁶It must be noted, however, that in single crystals of $\text{Ca}_3\text{Co}_2\text{O}_6$, there is a sizable difference between the magnetization values at low T (e.g., 2 K) and at intermediate T (e.g., 10 K), in the field range just above the main step on $M(H\parallel c)$ (see, for instance, Ref. 13).
- ⁴⁷T. Burnus *et al.* (private communication).